

Field-Scale Model for Air Sparging Performance Assessment and Design

G. Hein (email: glhein@mtu.edu)

N. Hutzler (email: hutzler@mtu.edu)

J. Gierke (email: jsgierke@mtu.edu)

Department of Civil and Environmental Engineering
and

Department of Geological Engineering and Sciences

Michigan Technological University

1400 Townsend Drive

Houghton, MI 49931-1295

R. Falta (faltar@clemson.edu)

Department of Earth Sciences

Brackett Hall, Box 341906

Clemson University

Clemson, SC 29634-1908

S. Giese (email: giese@caelab1.cae.wisc.edu)

Department of Civil and Environmental Engineering

University of Wisconsin-Madison

Madison, WI 53706

Research Sponsored by U.S. Department of Energy's Morgantown Energy Technology Center, under Contract Number: DE-RO21-95MC33082 with Michigan Technological University, 1400 Townsend Drive, Houghton, MI 49931-1295, telefax: (906) 487-3371

Contract Manager: Karl Heinz-Frohne

Introduction

Air sparging has been used as an *in situ* technique to remove VOCs (volatile organic compounds) from contaminated groundwater. Very few studies have been completed to quantify the remediation regime or the mass transfer processes. Figure 1 shows a typical air sparging field installation.

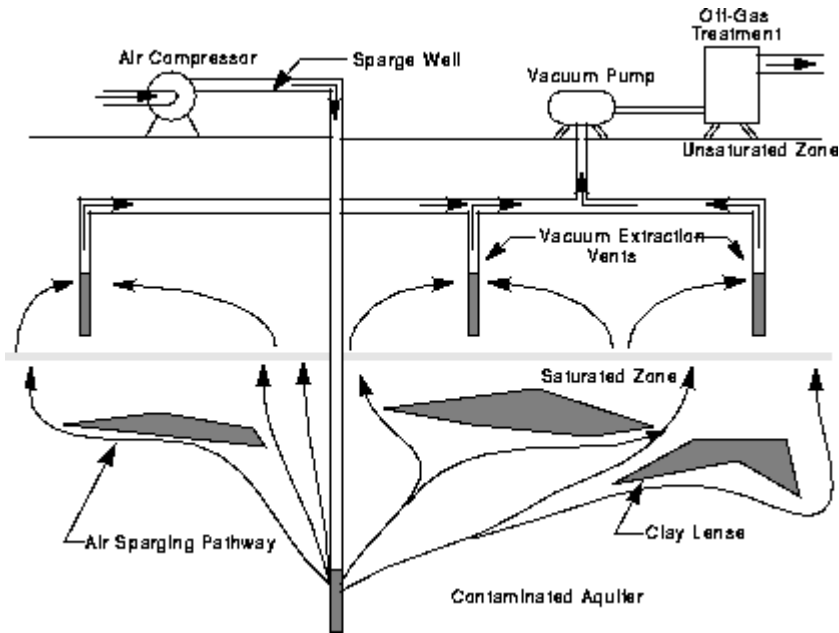


Figure 1: Air Sparging Field Schematic

As shown in this figure, air is injected into the groundwater from an injection well. The VOC partitions into the air phase and rises to the unsaturated zone. At this point, another technology, typically soil vapor extraction (SVE) is used to remove the gases from the vadose zone.

Problem

Existing methods used to estimate the effectiveness of air sparging and the time required for treatment are unrealistic because the flow and mass transfer processes are not well understood. Many existing models do not consider mass transfer processes or they define the air flow patterns insufficiently. Therefore, the time required for a site clean-up is underestimated, while extent of the air sparging regime is usually overestimated. A computer model that more accurately describes this process is needed to provide more realistic treatment estimates.

Solution

A logical sequence of experiments are being performed to identify the mechanisms controlling mass removal and to quantify their rates based on basic porous media and chemical properties and hydraulic characteristics. Modeling is being used to analyze the experimental results and to demonstrate the correct mechanistic approach that will be used in developing a field-scale performance assessment model. The field-scale performance assessment model will be tested against field data obtained under controlled conditions.

Project Description

To complement ongoing field and laboratory research into air flow patterns induced by air sparging, there is a critical need to perform controlled laboratory experiments to identify and quantify mass transfer rates for air sparging. This mechanistic study is being performed such that the results can be incorporated into existing theoretical frameworks for air flow patterns and eventually can be used for design guidance. Controlled experiments are needed because the important processes are not well understood nor even positively identified. This study of mass transfer processes includes a demonstration of the appropriate approach to model mass transfer. The theoretical model is used to help understand the laboratory results. A field-scale air sparging model is being developed to include mass transfer from the liquid phase to the gaseous phase so that it can simulate the removal of a VOC mixture composed of up to 10 components. The model output will show the extent of remediation, the air pressure distribution and saturation distribution. This information can be used to more accurately design an air sparging system or determine if air sparging is applicable under a given set of conditions.

To test the model, a series of column experiments are underway for three cases: single-solute, multi-solute and single-NAPL column experiments. The successful completion of the laboratory results is being established by comparing model predictions to the results. Two chemicals (trichloroethylene and toluene) are used in the experiments. At least five experiments are being performed with each (2 single-solute, 2 multi-solute, and NAPL phase).

The single-solute experiments were repeated for the following conditions: two different grain sizes and a distribution of grain sizes. The gaseous-phase emissions were monitored, and the contaminant mass removed was compared to the amount injected into the column. A residual amount of contaminant should remain in the column. Multi-solute experiments will be completed to see if there are compositional effects. The multi-solute experiments consist of a two-component mixture of TCE and toluene. The column experiments and modeling that have been completed to date are outlined in the following section.

The procedures for the single-NAPL experiments will be identical to dissolved solute experiments. A residual saturation of TCE and toluene will be used in these experiments. The

residual will be located in the upper portion of the saturated soil column. Tests will be repeated for several residual levels to determine if the mass transfer rate is a function of the amount of residual.

The final test of the model will involve comparing numerical results to field data generated during a pilot-scale air sparging/soil vapor extraction test. The field-scale tests are being performed under a separate award from the EPA. The tests were conducted in 3x5x8-m deep test cell at Hill AFB, Utah. The soil at Hill AFB is typical of most current sparging applications in that it has a high permeability. The primary contamination is jet fuel (JP-4) so the fullest capabilities of the model will be tested. The test cell was fully instrumented for pressure and concentration monitoring. Multiple test conditions were performed so there are more than one set of test results for model comparison.

Results

This project has been focussing on the completion of the laboratory work. To date we have completed the single solute experiments. The results are presented below. We have also been working on the modifications to the field-scale model (T2VOC). Some preliminary simulations are presented below.

Soil Column Experimental Apparatus

The soil column experiments were conducted to determine the rate of dissolved-phase VOC removal during air sparging. Each experiment was run in duplicate at an injection flowrate of 10 mL/min in a 5.0-cm diameter column containing Ottawa sand according to the schematic shown in Figure 2. Prior to the test, the column was uniformly packed in 0.5-cm lifts with US Standard No. 20 x 30 mesh Ottawa sand to a depth of 28-cm. The empty column mass and the mass of the column packed with dry sand were measured to calculate the bulk density and porosity. The column was saturated by circulating water through it overnight. Afterwards, the column was weighed to obtain the saturated soil mass. For the next 24 hours, nitrogen was injected through the bottom of the column to displace water and establish air channels. The flow was regulated using a micrometer valve (Swagelock M/N SS-21RS4, Appleton, Wisconsin). The flowrate was measured using a bubble meter (0 to 100 mL, Ace Glass, Vineland, New Jersey) located downstream of the soil column. The displaced water was collected in a beaker to check the degree of water saturation in the column. Afterwards, a nitrogen/methane mixture followed by a nitrogen/TCE mixture were fed through the column and to a gas chromatograph (GC) equipped with a thermal conductivity detector (TCD) (MTI M/N 200, Fremont, California) to measure the gaseous-phase concentration. The methane and TCE concentrations in the compressed gas cylinders were both 1000 ppmv, respectively (Matheson, Chicago, Illinois). Once the chemical concentration in the column effluent became constant, nitrogen was fed through the column to sparge the methane or TCE. The process was completed when the normalized concentration dropped to below the detection limit, which is approximately 10 ppmv. The column was weighed

after sparging to calculate the water saturation of the sand. After the test, the mass of water displaced was compared to the difference between the saturated column mass and the column mass after sparging. The difference between the two masses was less than 10 percent.

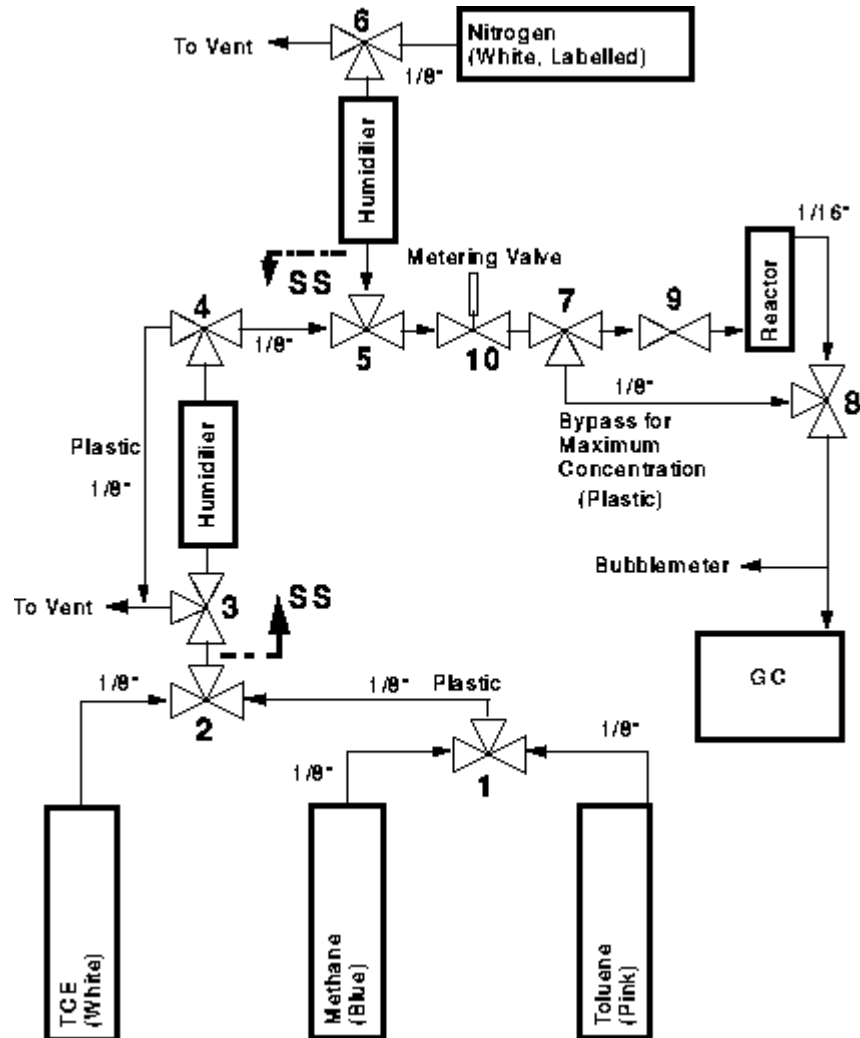


Figure 2: Diagram of Column Tests

Methane and TCE Soil Column Test Results

Measured retardations for the conservative tracer, methane, were within 10% of predicted retardations and are very reproducible (Table 1). Maximum concentration was attained at about three gas pore volumes and was stable until the sparging portion of the test began. Very little tailing was observed for either breakthrough or elution in any of the methane tests. Figure 3

shows the sparging curves for the six tests completed in June and July, 1997.

Measured retardations for the contaminant of interest, TCE, were lower than predicted. Retardation values for TCE are shown in Table 1. Although measured retardations were lower than predicted, the results were very reproducible. The data also suggests that increasing the column saturation will increase the retardation of TCE. This data trend corresponds to predicted effects of column saturation as shown in the retardation equation, which was discussed in the introduction. Sparging curves for TCE are included in Figure 4. The elution portion of the TCE tests noticeably tails for more than 20 or 30 pore volumes. Thus, it is possible that maximum concentration or complete TCE removal levels may have never been achieved. All six TCE tests exhibited this tailing phenomenon.

Measured retardation values were lower than predicted retardation values for the TCE tests. There may be at least two reasons for this result. One reason may be that TCE gas/water equilibrium was never reached in the column. Because retardation is high for TCE and liquid diffusion is a relatively slow mass transfer mechanism, equilibrium may take much longer to occur than assumed for these sparging tests.

The second reason may be due to a lack of sensitivity in the gas analysis. The GC used in these tests is not precise enough to adequately measure the TCE during the long concentration “tails”. If the GC could measure within five percent of the initial gaseous TCE concentration, C_0 , and the TCE tail was within five percent of C_0 , then the tail would be missed, and it would appear that equilibrium was reached (Gierke, 1997).

During the single-solute experiments, the GC method was changed to reduce variability in the TCE tail. The tailing trend for TCE was thought to be attributed to variability in GC readings. Thus, the method for analyzing TCE was changed by increasing the sampling time from 2 seconds to 10 seconds and by decreasing the run time from 120 seconds to 40 seconds. Also, the gas chromatograph was recalibrated using gas standards in Tedlar[®] bags. Tedlar[®] bags are gas-tight and can be filled or injected with gas through a valve on the bag. The calibration curve followed a linear regression over a 10 to 1000 ppm_v range. The detection limit was determined from the calibration curve to be approximately 10 ppm for both methane and TCE. The revised GC method had a negligible effect on TCE tailing.

Table 1: Experimental and Predicted Retardations for the Sparging Tests

	6/10/97	6/16/97	7/9/97	7/14/97	7/21/97	7/25/97
Dead Vol. (ml)	20	20	13.13	13.13	13.13	13.13
Flowrate (mL/sec)	0.21	0.22	0.19	0.19	0.28	0.27
Dia. of Column (cm)	5.01					
Area of Column (cm ²)	19.7					
Length of Soil Column (cm)	28.5					
Soil Type	20x30 Ottawa Sand					
Dry Bulk Density (g/cm ³)	1.62					
Porosity	0.34					
Initial Saturation	0.95		0.80		0.80	
Final Saturation	0.75		0.71		0.70	
Methane Predicted Retardation	1.11		1.09		1.09	
Methane Measured Retardation	1.10	1.15	1.04	1.11	1.15	1.13
TCE Predicted Retardation	9.43		8.13		7.73	
TCE Measured Retardation	4.14	4.43	3.38	3.18	3.48	3.20

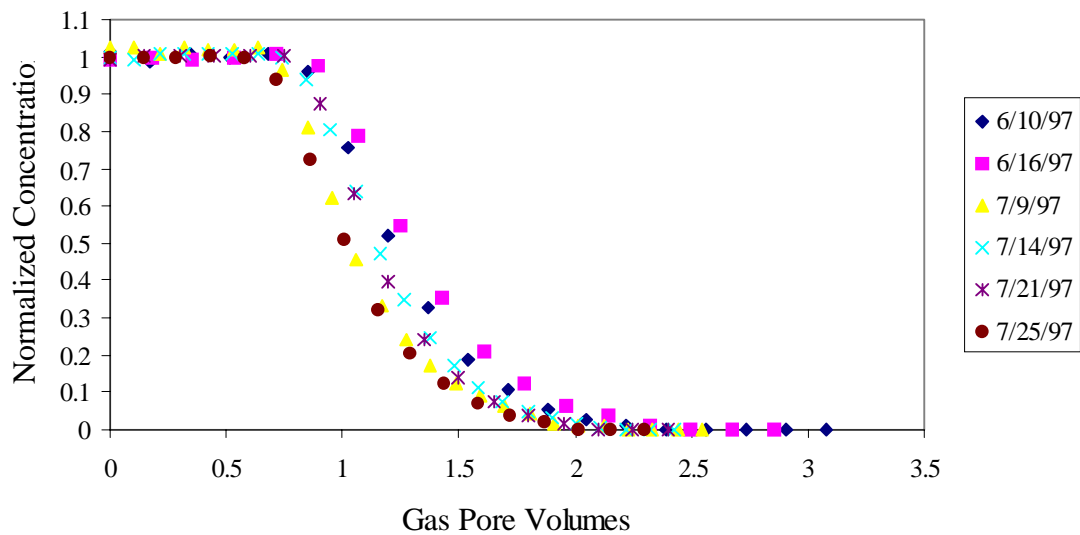


Figure 3: Laboratory Column Data for the Removal of Methane during Air Sparging

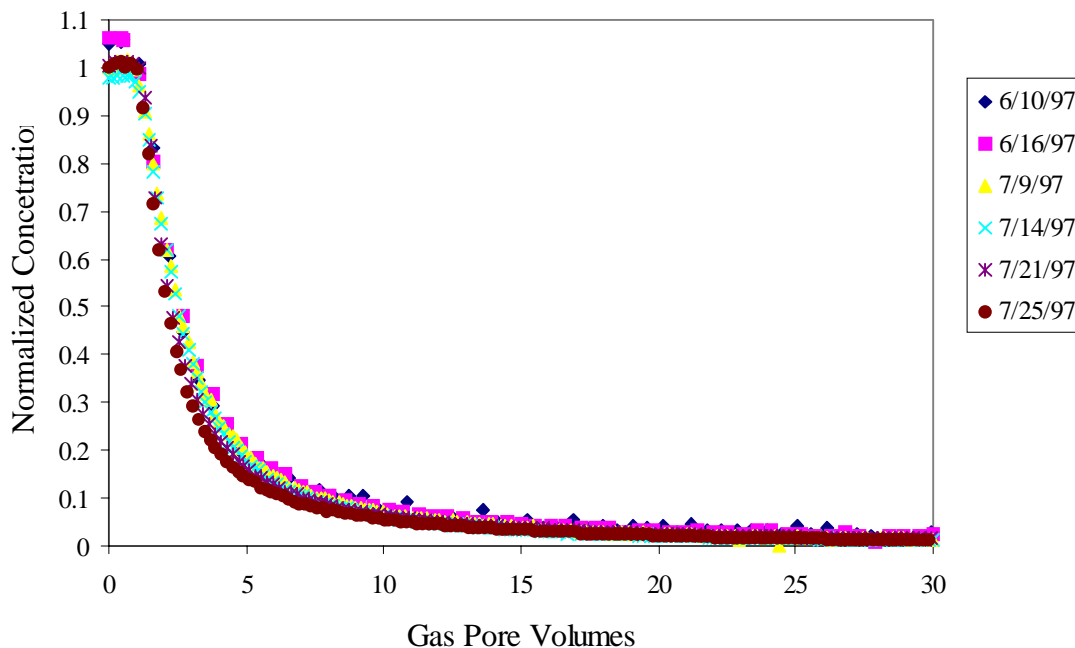


Figure 4: Laboratory Column Data for the Removal of TCE during Air Sparging

Modeling Rate Limited Mass Transfer During Air Sparging

Recent studies have clearly demonstrated that VOC removal during air sparging is limited by mass transfer into the flowing gas phase. These mass transfer limitations occur at several scales due to the heterogeneous nature of gas distributions during air sparging. At a large scale, the air sparging zone is very strongly influenced by heterogeneities which form capillary and permeability barriers to the gas flow. If the geometry and locations of these heterogeneities are well known, or if the media is homogeneous, it is possible to accurately model the sparge gas flow field using a conventional multiphase flow numerical approach (Hein et al., 1997; McCray and Falta, 1997).

Due to the unstable nature of air sparging gas flows, the gas tends to flow locally through small channels, which are separated by a distance of one or several millimeters. As mentioned above, it is possible to model the average effect of these local flows using a conventional local equilibrium approach with a multiphase flow simulator. This type of simulator, however, cannot resolve local mass transfer effects that arise due to the millimeter scale gas channels that form

during sparging. For this reason, compositional multiphase flow simulators that assume local chemical equilibrium between the phases overestimate the rate of contaminant removal during air sparging.

We propose a new method for modeling the local mass transfer during air sparging. This new technique is straightforward, and can be easily implemented in existing compositional multiphase flow simulators. The method is based on a dual-media formulation, which is commonly used for modeling flow and transport processes in fractured media [see Pruess and Narasimhan, 1985]. Instead of considering fractures and matrix blocks, the method is applied to porous media to simulate the local gas channels that form during air sparging. This allows us to resolve the local mass transfer limitation between the flowing gas phase, and nearby stagnant water filled zones. Compared to the usual local equilibrium approach, the dual media approach only doubles the number of equations to be solved at each time-step.

Figure 5 shows a schematic diagram of the dual media formulation. Each “normal” gridblock is subdivided into two media. In the classical application of this method, these media would be fractures and matrix, and the fracture spacing would typically be on the order of one to several meters. The two media are connected inside the gridblock by a single one-dimensional connection, with a single average interfacial area between the two media in the gridblock. The average distance between the two media, and the average interfacial area is computed based on the distributions of the two media within the gridblock (the three-dimensional fracture spacing in the fractured rock case). Each dual media gridblock is connected to other gridblocks in the normal way, but with connections for both media [Pruess and Narasimhan, 1985]. Thus the method can be applied to complex 3-D grids if desired.

In the present application, we consider two types of porous media: a high permeability, low capillary pressure media (coarse sand for example), and a lower permeability, higher capillary pressure media (a medium sand for example). Compared to fractured rock applications, we assume a much smaller spacing between the two media, with a correspondingly larger interfacial area. For the case shown in Figure 5, the high permeability zones are separated by only 5 mm, so the average distance from the high permeability to the low permeability zones is only a millimeter or so, depending on the geometric model. The average interfacial area is very high in this case, approximately 768 m^2 of interface per m^3 of porous media.

The properties of the two media, and their distributions are chosen so that the sparging gas will form the characteristic local channels through the high permeability media. Currently, we do not have a technique for determining these parameters based on traditional porous media measurements, and rely instead on fitting. This is a significant limitation to the method, and it is an area where further research could provide important practical developments.

Dual Permeability Grid

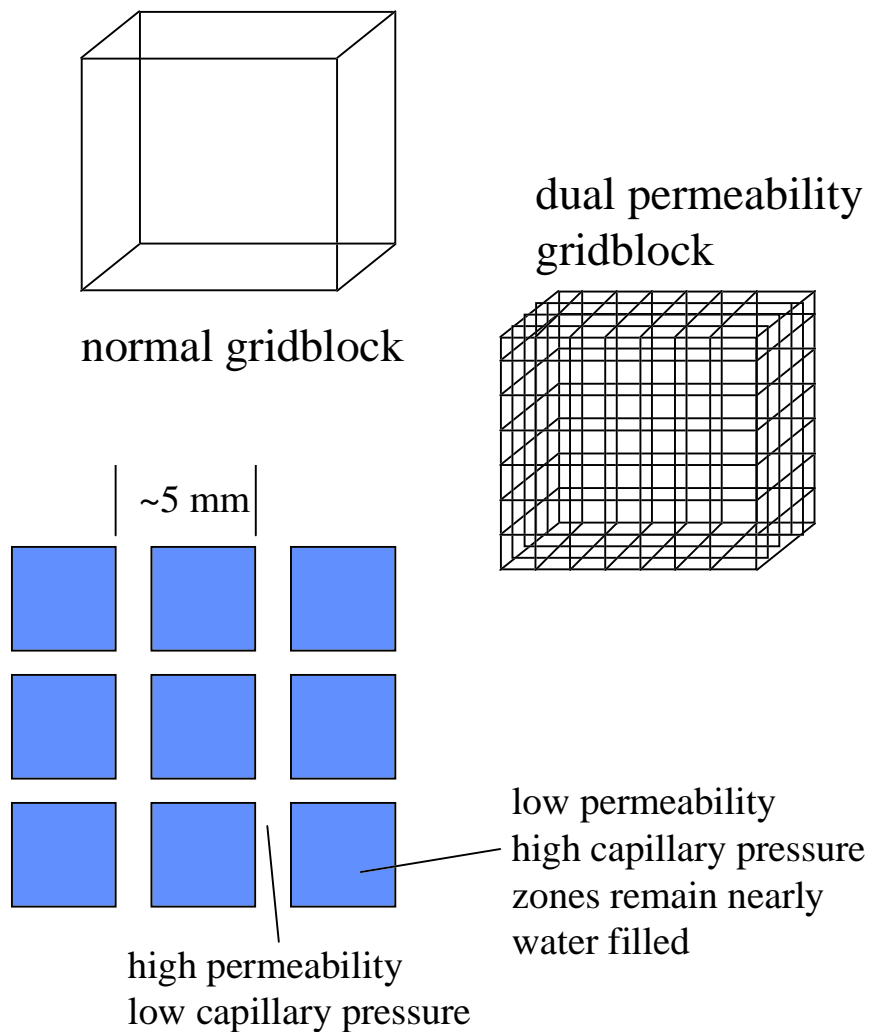


Figure 5: Schematic diagram of the dual media approach for modeling air sparging. The two media are only represented by two nodes in each volume element, with one node representing the high permeability zone, and the other representing the low permeability zone.

During an air sparging simulation, almost all of the gas flows through the high permeability/low capillary pressure zone. Considering an initially contaminated zone, the high rate of gas flow quickly removes the contaminant from the high permeability zone. This gives rise to a diffusive gradient from the nearly water filled low permeability zone towards the gas filled high permeability zone (Figure 6). Because each media is modeled with a single node separated by some average distance, this diffusive mass transfer is mathematically analogous to a first-order interphase mass transfer reaction:

$$Q_{int}^c = K_{int} (C_{w,l}^c - C_{g,h} / H)$$

where Q_{int}^c is the rate of chemical transfer from the low permeability media to the high permeability media per unit volume, $C_{w,l}^c$ is the aqueous phase chemical concentration in the low permeability media, $C_{g,h}^c$ is the gas phase chemical concentration in the high permeability media, and the mass transfer coefficient, K_{int} includes both liquid and gas phase diffusion:

$$K_{int} = \frac{(\phi S_g \tau_g D_g H + \phi S_w \tau_w D_w) A}{d}$$

where $\phi S_g \tau_g D_g$ is an effective porous media diffusion coefficient, A is the average interfacial area between the two media per unit volume of porous media, and d is the average distance between the two media.

A series of simple numerical simulations were performed to illustrate the method. These were conducted using the three-dimensional T2VOC compositional multiphase flow simulator [Falta et al., 1995], modified to account for aqueous phase diffusion. This code already contains a provision for modeling dual media problems. The simulations model two hypothetical column air sparging tests, one with dissolved TCE, and one with separate phase TCE (DNAPL).

In the first set of simulations, air containing 35 mg/l of TCE vapor is injected into the bottom of a vertical water filled column. As the system equilibrates, the gas flow stabilizes, and the pore water becomes contaminated at a concentration of about 100 mg/l. This provides the initial conditions for the TCE removal simulation, which consists of the injection of clean air at a darcy velocity of 0.001m/s or about one pore volume every 400 seconds. The numerical and porous media parameters used in the simulations are shown in Table 2. Based on the computed phase saturations, the effective interphase mass transfer coefficient, K_{int} is about 4×10^{-4} /s for these simulations. This quantity is dynamic, however, and is continuously changing as gridblock conditions change.

Mass transfer model inside each gridblock

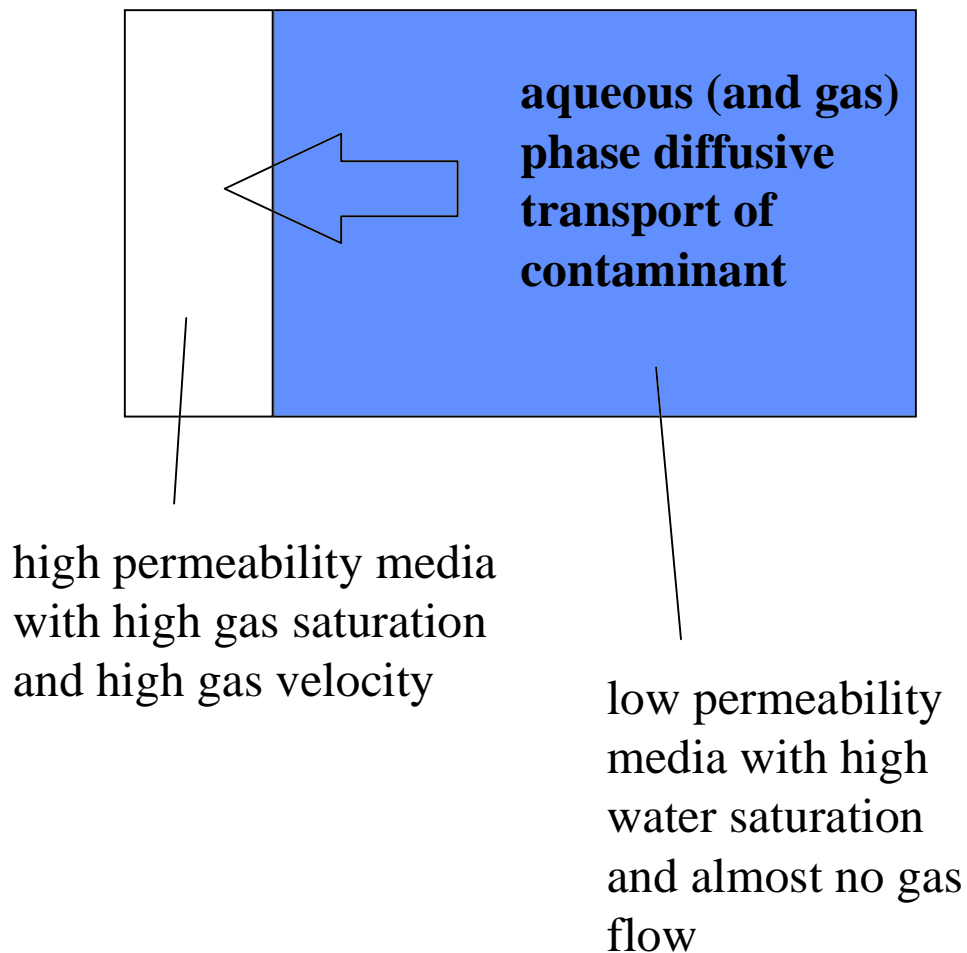


Figure 6: Schematic diagram of the local mass transfer inside each dual media gridblock. The contaminant diffuses from the high water saturation low permeability zone into the gas filled high permeability zone.

Table 2: Parameters used in 1-D Simulations of a One Meter Long Column

	Local Equilibrium Model with normal gridblocks	Dual Media Approach	
		High Permeability Zone	Low Permeability Zone
Gridblock Spacing	0.1m (10 gridblocks)	0.1m (10 gridblocks)	0.1m (10 gridblocks)
Permeability	42.4 darcies (effective average of the dual media)	100 darcies	10 darcies
van Genuchten capillary pressure parameter, α	10.27m ⁻¹ (volume weighted average of the dual media)	15.8 m ⁻¹	5.0 m ⁻¹ (using Leverett scaling with the permeability)
Dual Media Volume Fractions	Not Applicable	0.488	0.512
Dual Media A/d	Not Applicable	1.229x10 ⁶ m ⁻²	1.229x10 ⁶ m ⁻²

Figure 7 shows the computed effluent concentrations from the column as a function of time. The local equilibrium model (the curve labeled C_g(single)) produces a classical advection/diffusion breakthrough curve, with very little tailing. The mass transfer model (the curve labeled C_g(dual)), on the other hand, shows a much quicker decline in effluent concentration, followed by a long period of tailing. This behavior is typical of real experiments, which almost always show these strong mass transfer effects. It is important to note here that the dual media simulation only used 20 gridblocks, compared to 10 for the local equilibrium case. Because the increase in the number of equations only doubles with this approach, it is practical for 3-D field scale simulations.

Figure 8 shows the gas concentration profile in the column after 700 seconds. This figure illustrates the degree by which the two media in the dual media approach are out of equilibrium. At this time, there is a strong mass transfer from the low permeability zone to the high permeability zone. Because almost all of the gas is flowing through the high permeability zone, the effluent concentration from the dual media simulation is lower than the effluent concentration from the single media case at this time.

The second simulation case involved liquid TCE (DNAPL). In this case, the DNAPL was uniformly mixed (both media in other words) in the bottom 90 cm of the column, with an initial saturation of 10%. This is below the NAPL residual saturation in the model, so the DNAPL is immobile. The simulations are conducted as before, with clean air injected into the bottom of a

liquid filled, vertical column.

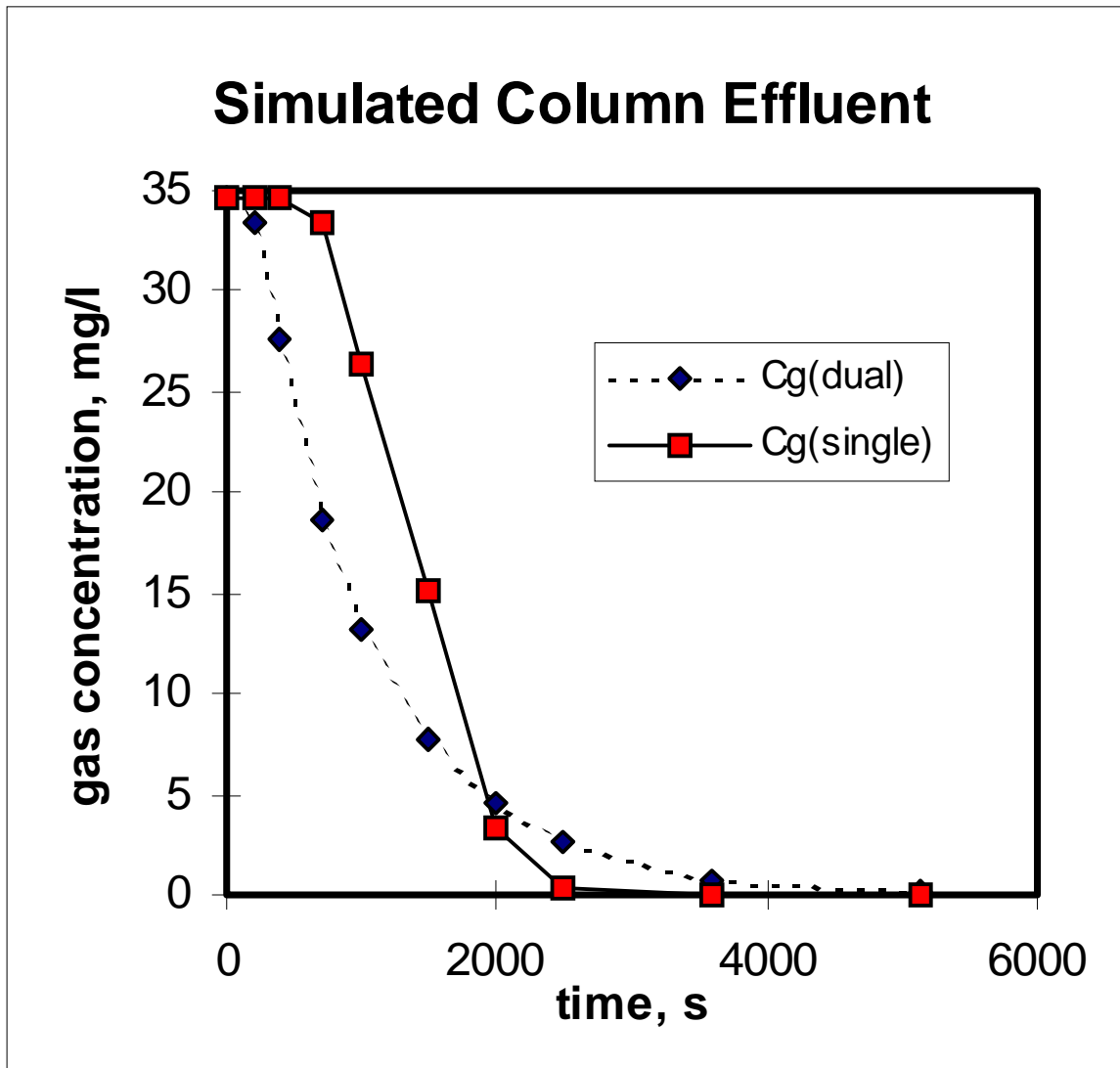


Figure 7: Comparison of the effluent concentrations from dual media mass transfer model to a conventional local equilibrium model for a column air sparging case.

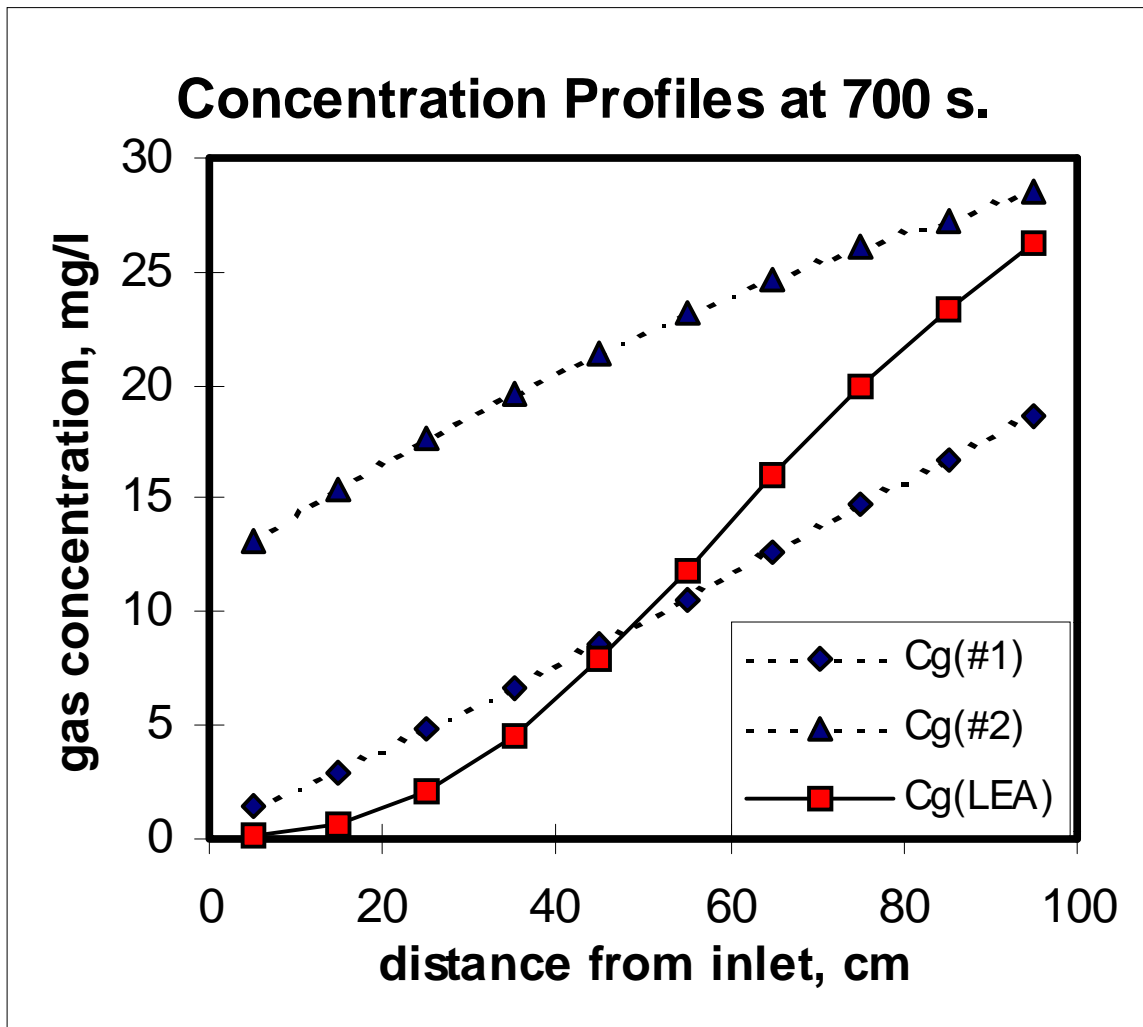


Figure 8: Computed gas concentration profiles inside a simulated air sparging column. The curves Cg(#1) and Cg(#2) refer to the low permeability and high permeability parts of the dual media gridblocks. Note that the two media are far from equilibrium at each position in the column.

Figure 9 shows the simulated column effluent for the two modeling approaches. Using the normal local equilibrium model, the effluent gas concentration remains at the saturated TCE vapor concentration until all of the DNAPL has evaporated, at which time it suddenly drops to zero. The dual media case, on the other hand, shows a more gradual decline in effluent concentration with time. The initial drop in concentration occurs when the DNAPL evaporates out of the high permeability zone. This leads to a mass transfer limited evaporation and dissolution of the

DNAPL from the lower permeability zone, where little gas flow occurs. As the DNAPL is gradually removed from the low permeability gridblocks near the air injection point, the overall mass flux into the high permeability zone decreases, causing a reduction in the effluent concentration.

Figure 10 shows the NAPL saturation profile in the column after one day of air injection. The local equilibrium case (Sn(LEA)) shows a very sharp evaporation front at about 60cm. In this case, all of the mass transfer instantly occurs at this front. The dual media case is quite different. At this time, all of the DNAPL in the high permeability zone has evaporated, and the DNAPL in the low permeability zone is slowly evaporating and dissolving and diffusing into the high permeability zone.

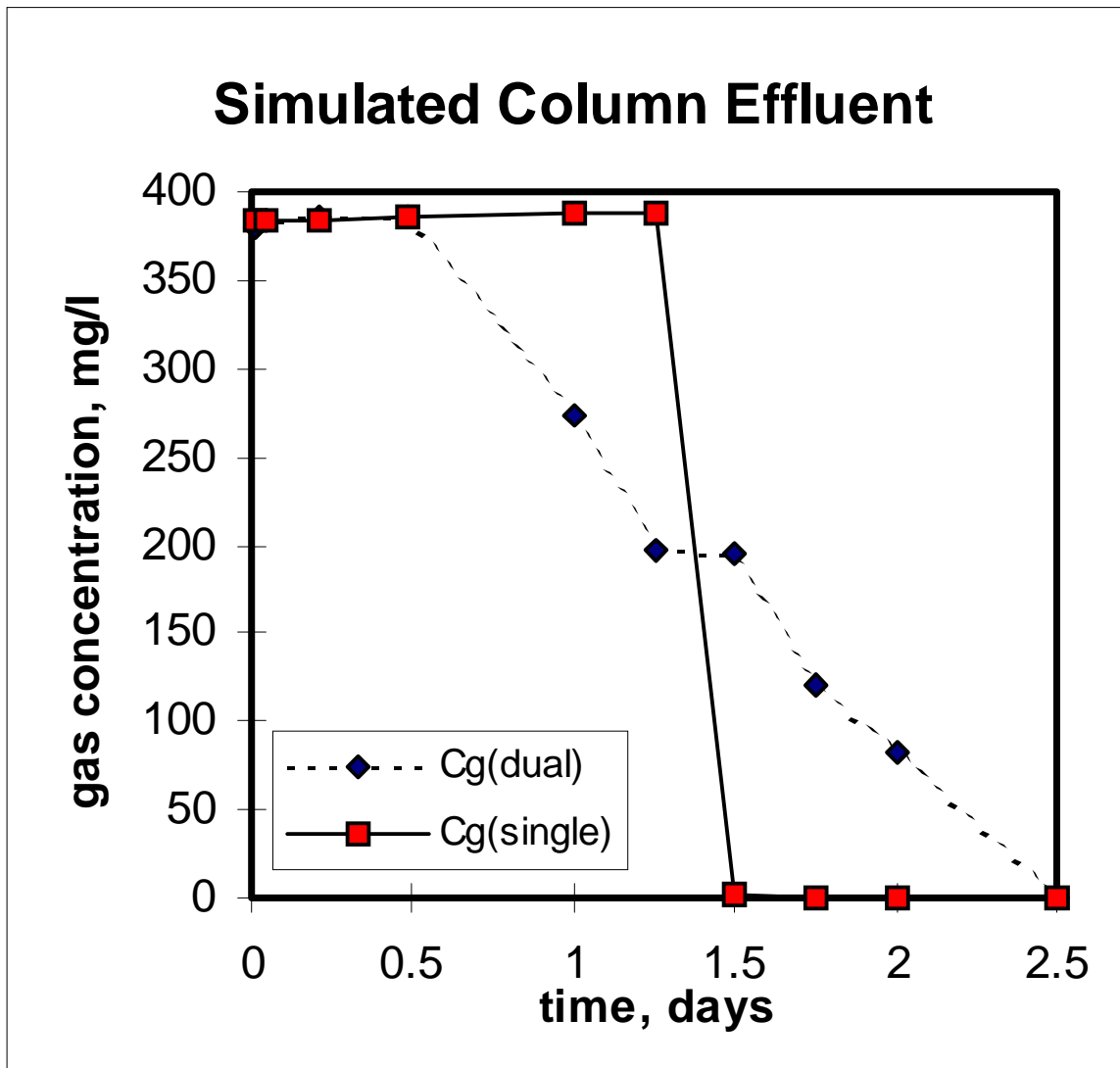


Figure 9: Comparison of simulation results for an air sparging column containing TCE in the form of a NAPL. The $C_g(\text{single})$ curve represents the traditional local equilibrium approach, while the $C_g(\text{dual})$ curve is calculated using the dual media concept.

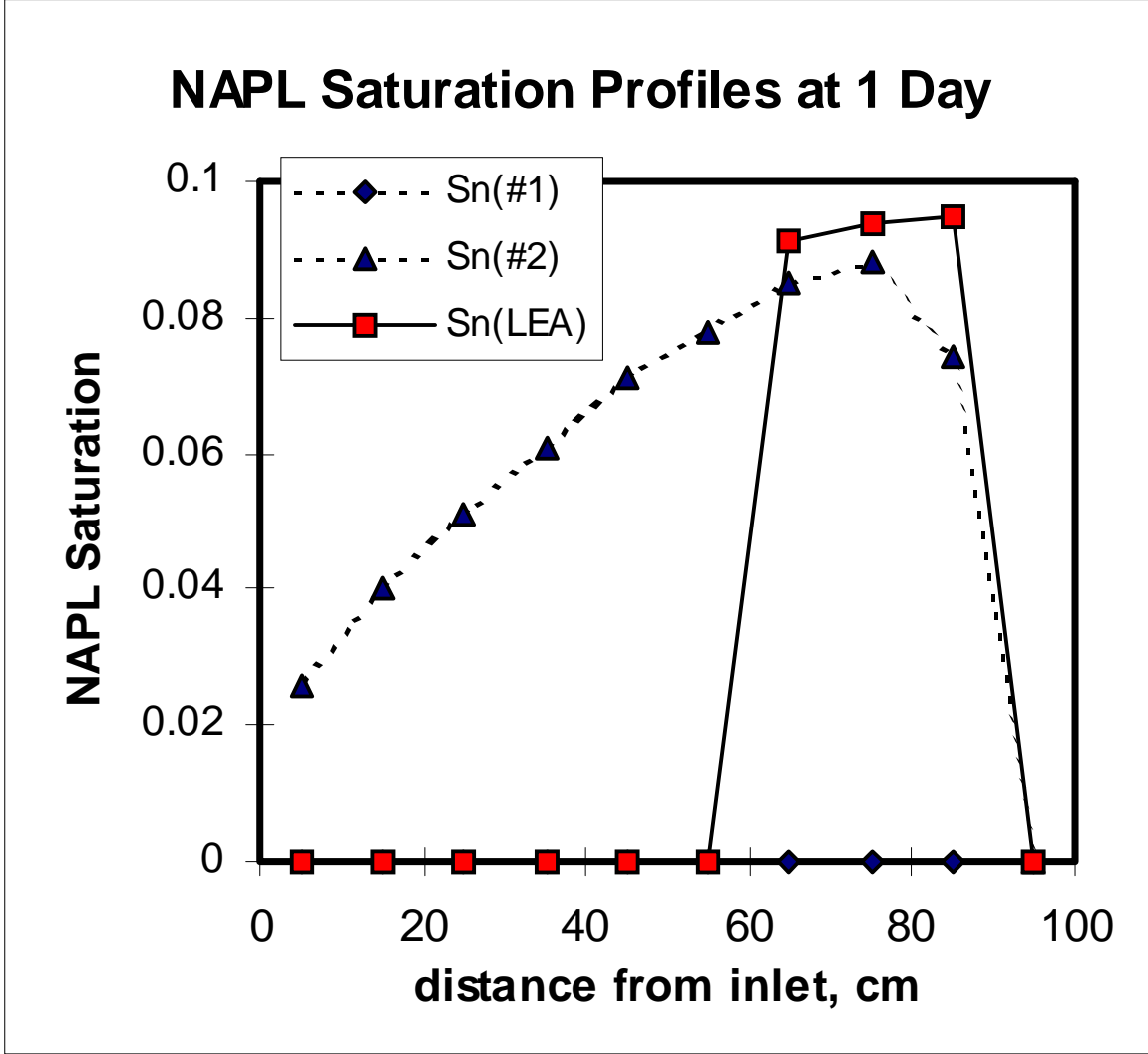


Figure 10: Computed NAPL saturation profiles in a hypothetical air sparging column. The Sn(LEA) curve corresponds to the local equilibrium approach. The Sn(#2) curve corresponds to the low permeability media using the dual media approach. At this time, all of the NAPL has evaporated from the high permeability media (curve Sn(#1)).

Application/Benefits

Since the primary goal of this project is to obtain a greater understanding of the mass transport mechanisms involved in air sparging, we plan to provide documentation to aid in the design and application of this technology by:

- Developing a field-scale air sparging model to obtain more effective treatment, more realistic estimates of remediation times and improved design configurations
- Providing design guidance for air sparging that takes into consideration the impacts of mass transfer.
- Providing guidance for conducting laboratory tests of and developing mechanistically correct models for air sparging tests.

These deliverables will aid engineers and scientists in the design and implementation of air sparging systems. They will also indicate which design parameters have the greatest impact on air sparging operation.

Future Activity

This project is composed of two sections: model development and laboratory experiments. These parts are being completed independently. Then model testing is conducted using the laboratory data. The final model testing will be done by comparing numerical predictions to data obtained from a field site. When these tasks are finished, a users manual will be written such that engineers can use this code to predict the performance of an air sparging system at field sites and in the laboratory. The model development is being completed at Clemson University, while the laboratory testing and field data is being completed under the direction of Michigan Technological University.

Acknowledgments

We would like to thank the U.S Department of Energy for funding this research and Karl Frohne, the METC Contracting Officer's Representative for his guidance on this project. This research began in August 1996 and will be completed in 1998. We also appreciated the modeling that Heidi Grenkowitz, a graduate student at Michigan Technological University completed.

References

Falta, R.W., K. Pruess, S. Finsterle, A. Battistelli, T2VOC User's Guide. Lawrence Berkley Laboratory, Report LBL-36400, March, 1995, pp. 1-155.

Gierke, J.S., N.J. Hutzler, J.C. Crittenden, "Modeling the Transport of Volatile Organic Chemicals in Unsaturated Soils," WRR, Vol. 26, No.7, 1990, pp.1529-1547.

Gierke, J.S., N.J. Hutzler, D.B. McKenzie, "Vapor Transport in Unsaturated Soil Columns: Implications for Vapor Extraction". WRR, Vol. 28, No. 2, 1992, pp. 323-335.

Hein, G.L., J.S. Gierke, N.J. Hutzler, R.W. Falta, "Three-Dimensional Experimental Testing of a Two-Phase Flow-Modeling Approach for Air Sparging". GWMR, Summer, 1997, pp. 222-230.

Hein, G.L., N.J. Hutzler, J.S. Gierke, "Quantification of the Mechanisms Controlling the Removal Rate of Volatile Contaminants by Air Sparging", Proceedings of the 1994 National Conference on Environmental Engineering on Critical Issues in Water and Wastewater Treatment, ASCE, Environmental Engineering Div., Boulder, CO, July 11-13, 1994.

Hunt, J. R. et al. (1988). "NAPL Transport and Cleanup, I. Analysis of Mechanisms." WRR, **24**, (8), pp. 1247-1258.

Ji, W., A. Dahmani, D.P. Ahlfeld, J.D. Lin, E. Hill, III, "Laboratory Study of Air Sparging: Air Flow Visualization". GWMR, Fall, 1993, pp. 115-126.

McCray, J.E., Numerical Analysis of Air Sparging for Subsurface Remediation. Masters Thesis, Clemson University, 1994.

McCray, J.E., R.W. Falta, "Numerical Simulation of Air Sparging for Remediation of NAPL Contaminaton". Groundwater, **35**, (1), pp. 99-110.

Microsensor Technology, Inc., EZ Chrom 20 Chromatograph Data System, Operators Manual. P/N 20049, 1990.

Microsensor Technology, Inc., M200 Operations Manual. P/N 20050, 1990.

Millington R.J., J.P. Quirk, "Permeability of Porous Solids". Trans. Faraday Soc., **57**, pp. 1200-1207.

Pruess, K. and T. N. Narasimhan, "A practical method for modeling fluid flow and heat flow in fractured porous media". Soc. of Petroleum Eng. Journal, 25(1), Feb., 1985, pp.14-26.